Progress In Electromagnetics Research M, Vol. 114, 153–163, 2022

SbD Synthesis of Dual-Band Perturbed Minkowski Monopole Fractal Antennas

Lorenzo Poli* **and Arianna Benoni**

Abstract—An innovative methodology for the design of dual-band microstrip monopole antennas is presented in this work. It leverages on the unconventional modeling of the radiator shape based on the perturbed Minkowski fractal in order to fit arbitrarily-defined resonances. A System-by-Design (*SbD*) technique is exploited to solve the arising global optimization problem with high computational efficiency. Representative benchmarks are reported to assess the effectiveness, reliability, and efficiency of the proposed synthesis approach.

1. INTRODUCTION

The rapid development of the Internet-of-Things (*IoT*) and the Internet-of-Everything (*IoE*) is causing an exponentially-growing need for small-size, cheap, and densely interconnected wireless devices capable of "pervasive intelligence" [1, 2]. One pillar asset supporting such a technological advancement is represented by the design of compact and low-profile *IoT/IoE* devices simultaneously supporting heterogeneous wireless standards and services (e.g., *LTE, WLAN, UMTS, Bluetooth, GPS*, *RFID*) [1]. Such a necessity has been driving during the last decade a remarkable interest in the design of innovative multi-band antennas (*i*) simultaneously transmitting/receiving electromagnetic (*EM*) energy within different portions of the spectrum and (*ii*) enabling a miniaturization of the radio-frequency (*RF*) front-end [3–6]. In such a framework, fractal antennas are considered an effective and versatile recipe to implement low-profile radiating structures naturally exhibiting different scales of detail that are independently excited at different wavelengths of the *TX/RX* signal [7–14]. However, designs based on conventional fractal shapes, whose geometry descriptors are derived by means of iterative analytical relationships, generally exhibit fixed-ratio locations of the working resonances [7, 8]. To overcome such a limitation, radiators based on "perturbed" fractal shapes have been introduced, proving an increased flexibility in their resonance behavior and enabling the implementation of multi-band devices hosting arbitrary wireless standards [15–17]. Nevertheless, the "price to pay" is an increased complexity of the synthesis problem due to the larger number of design variables and the unavailability of closed-form formulas to determine non-uniform heterogeneous-scale details. Therefore, the design of perturbed fractals often relies on global optimization techniques such as evolutionary algorithms (*EA*s) for an effective exploration of the solution space without requiring the analytical knowledge of the cost function derivative nor suffering from its multi-modal nature [15–21]. Unfortunately, directly integrating *EA*s with accurate but time-consuming full-wave (*FW*) *EM* solvers for assessing the fitness of each trial design turns out to be computationally cumbersome, easily yielding long synthesis times [15].

To overcome such an issue, several synthesis methodologies have been recently developed within the artificial intelligence (*AI*) and machine learning (*ML*) frameworks in order to alleviate the computational complexity while guaranteeing effective solutions [22–26]. In this context, the System-by-Design (*SbD*)

Received 18 June 2022, Accepted 21 July 2022, Scheduled 24 November 2022

* Corresponding author: Lorenzo Poli (lorenzo.poli@unitn.it).

The authors are with the ELEDIA Research Center (ELEDIA@UniTN — University of Trento), DICAM — Department of Civil, Environmental, and Mechanical Engineering, Via Mesiano 77, 38123 Trento, Italy.

recently emerged as a *functional eco-system* to handle complexity in *EM* design problems by means of properly selected, implemented, and interconnected functional blocks depending on the objectives, constraints, and degrees-of-freedom (*DoF*s) at hand [27, 28]. Several implementations of the *SbD* have been proposed for the robust and cost-efficient synthesis of different *EM* devices including radomes [28], reflectarrays [29], wide-angle impedance layers (*WAIM*s) [30–33], metamaterials [34], polarizers [35], and *EM* skins [36, 37]. Concerning the design of fractal antennas, a pioneer attempt to apply the *SbD* to the synthesis of Sierpinski Gasket radiators has been presented in [15] based on Orthogonal Arrays (*OA*s), Support Vector Regression (*SVR*), and Particle Swarm Optimization (*PSO*). Although such a technique proved to be effective and computationally convenient over a standard *EA*-based optimization, it lacks any possibility to control the "degree of reliability" of the predictions outputted by the *SVR* during the optimization process, thus not guaranteeing *a-priori* that the final solution will be fully compliant with the project requirements [15]. Differently, this work investigates the suitability of a recently-proposed *SbD* algorithm based on the "interactive collaboration" between a *PSO*-based Solution Space Exploration (*SSE*) block and a fast Surrogate Model (*SM*) relying on the Ordinary Kriging (*OK*) *ML* technique [23, 27]. Thanks to the capability of the *OK* to provide the *SSE* block with an estimation of the confidence level of its predictions, properly-chosen trial solutions are selected and *FW*-simulated to adaptively enhance the *SM* accuracy during the optimization [27]. Such a *SbD* strategy is here applied, for the first time to the best of the authors' knowledge, to the expedite design of low-profile dual-band monopole antennas with arbitrarily-located resonances. Towards this end, a novel perturbed Minkowski monopole (*PMM*) modeling is proposed to derive, in combination with the *SbD* solution engine, an effective, robust, and efficient design methodology for the synthesis of dual-band radiators with the user desired *EM* behavior.

2. *SBD*-DRIVEN SYNTHESIS OF DUAL-BAND *PMM* RADIATORS

The geometry of the proposed dual-band *PMM* is sketched in Fig. 1. The antenna is realized in printed circuit board (*PCB*) technology by etching a rectangular ground plane of height H_g [Fig. 1(b)] on the bottom face and the fractal-shaped metallization on the top face of a dielectric substrate of relative permittivity ε, loss tangent $\tan\delta$, and thickness η [Fig. 1(a)]. To guarantee a proper input impedance matching over the target frequency bands, a tapered microstrip line of length H_f with bottom and top widths set to W_{f1} and W_{f2}, respectively, is used to feed the main radiator. As for this latter, it

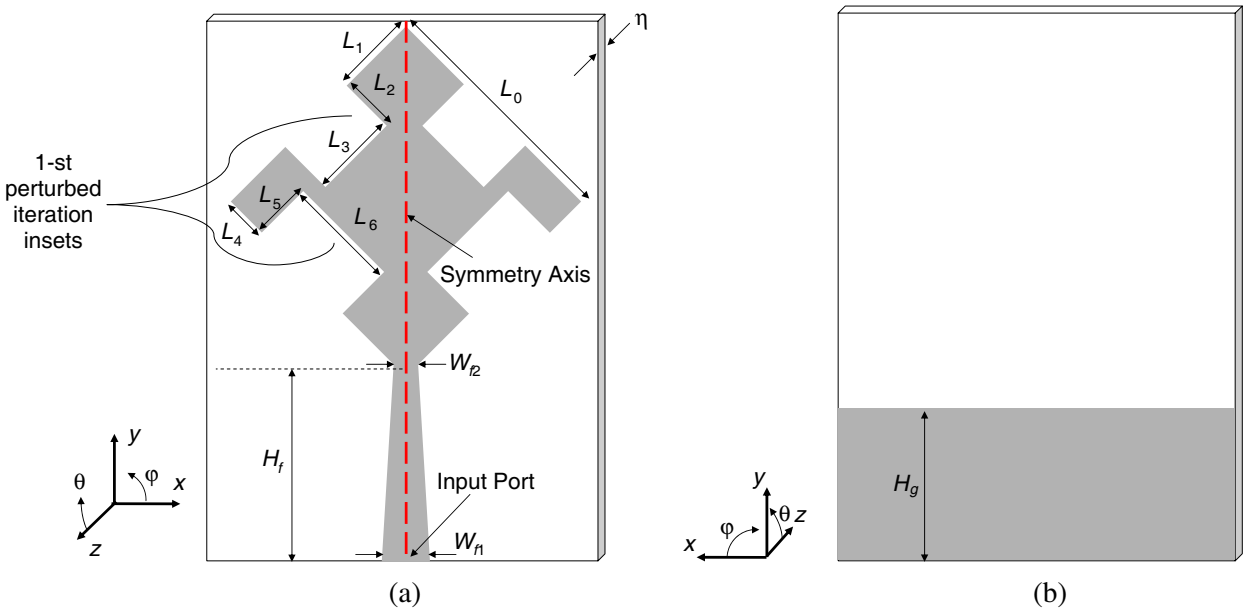

Figure 1. (a) Front and (b) back geometry sketches of the dual-band *PMM* radiator.

is modeled starting from a square microstrip patch of side L_0, implementing the 0-th iteration of the fractal shape, and therefore being mainly responsible of the fist (lower-band) resonance. As for the 1-st perturbed Minkowski fractal iteration, four non-uniform rectangular insets/indentations are etched from the square patch to realize the desired second (higher-band) resonance by introducing arbitrarily-shaped higher-scale details [Fig. 1(a)]. To yield a symmetrical pattern in the horizontal plane (i.e., $\varphi = 0$ [deg]), the geometrical symmetry of the radiator is enforced by mirroring such insets with respect to the vertical (y) axis [Fig. 1(a)]. Accordingly, the *PMM* radiating surface is fully controlled by the set of $U = 7$ geometrical descriptors $\underline{L} = \{L_u;\, u = 0, ..., U-1\}$ [Fig. 1(a)]. It is worth remarking that such an unconventional modeling is aimed at overcoming the fixed relation between successive resonances imposed by the canonical Minkowski fractal shape [13, 14], thus enabling the effective design of monopole antennas with uncorrelated resonance locations.

Owing to the proposed modeling of the radiator shape, the dual-band *PMM* accounts for $K = 11$ *DoF*s, i.e., (Fig. 1)

$$\underline{\chi} = \{\chi_k;\, k = 1, ..., K\} = \{H_g,\, H_f,\, W_{f1},\, W_{f2},\, \underline{L}\}\,. \tag{1}$$

Due to the unavailability of analytical formulas to derive the set of *PMM* descriptors enabling arbitrarily-defined resonances, the synthesis problem at hand is formulated as a global optimization one aimed at retrieving the optimal set of *DoF*s as

$$\underline{\chi}^{(opt)} = \arg\left[\min_{\underline{\chi}} \Phi\left\{\underline{\chi}\right\}\right] \tag{2}$$

where $\Phi\{\cdot\}$ is the cost function defined as the mismatch between the *FW*-computed $[S_{11}(f_{b,n}|\,\underline{\chi})]$ and target (S_{11}^{th}) dB-scale input reflection coefficients

$$\Phi\left\{\underline{\chi}\right\} = \sum_{b=1}^{B}\sum_{n=1}^{N_b} \mathcal{H}\left\{\frac{S_{11}\left(f_{b,n}|\,\underline{\chi}\right) - S_{11}^{th}}{\left|S_{11}^{th}\right|}\right\}. \tag{3}$$

In (3) B is the number of resonating bands (i.e., $B = 2$), and

$$f_{b,n} = f_{b,\min} + (n-1) \times \frac{\Delta f_b}{(N_b - 1)} \tag{4}$$

is the n-th ($n = 1, ..., N_b$) frequency sample within the b-th ($b = \{1;\, 2\}$) band of extension $\Delta f_b = (f_{b,\max} - f_{b,\min})$, $f_{b,\min}$ and $f_{b,\max}$ being the corresponding minimum and maximum resonant frequency, respectively. Furthermore, $\mathcal{H}\{\cdot\}$ in Equation (3) is defined for a generic input α as $\mathcal{H}\{\alpha\} = \alpha$ if $\alpha > 0$, $\mathcal{H}\{\alpha\} = 0$ otherwise.

In order to effectively and efficiently deal with the global minimization problem (2) at hand, a suitably customized implementation of the *SbD* is exploited. More specifically, the adopted synthesis strategy relies on a *SSE* block based on the *PSO* and a computationally-fast *SM* $\widetilde{\Phi}\{\cdot\}$ of the exact (but time-consuming) cost function (3). Following the guidelines in the reference literature [27], the Ordinary Kriging (*OK*) [23] is chosen to build $\widetilde{\Phi}\{\cdot\}$ starting from a training set $\mathbb{T} = \left\{(\underline{\chi}_t;\, \Phi\left\{\underline{\chi}_t\right\});\, t = 1, ..., T_0\right\}$ of T_0 off-line-generated examples of (3), $\left\{\underline{\chi}_t;\, t = 1, ..., T_0\right\}$ and $\left[\Phi\left\{\underline{\chi}_t\right\};\, t = 1, ..., T_0\right]$ being input samples (i.e., *PMM* trial geometries) generated by means of the Latin Hypercube Sampling (*LHS*) strategy and the associated cost function values computed by means of *FW* simulations, respectively. According to the "confidence-enhanced" *PSO-OK* (*PSO-OK/C*) *SbD* approach [27], an adaptive *ML* strategy is implemented to progressively update the *SM* during the iterative optimization ($i = 1, ..., I$, I being the number of iterations) by *FW*-simulating and adding to $\mathbb{T}$ a set of $T_{upd} \leq I$ properly-chosen trial solutions in order to improve the prediction accuracy and enable a more reliable converge towards $\underline{\chi}^{(opt)}$. Thanks to such a *SbD* strategy, the time saving with respect to a standard global optimization (i.e., relying exclusively on iterated *FW* assessments of the cost function [16, 17]) turns out to be $\Delta t = \frac{(P \times I) - (T_0 + T_{upd})}{(P \times I)}$, P being the swarm size [27].

3. NUMERICAL ASSESSMENT

This section is aimed at assessing the capabilities of the proposed methodology for the synthesis of dual-band radiators with arbitrarily-located target resonances. Towards this end, let us consider in the following a first benchmark concerned with the design of a *PMM* simultaneously operating in the *LTE-1800* ($[f_{1,\min}, f_{1,\max}] = [1.71, 1.88]$ [GHz] $\rightarrow \Delta f_1 = 0.17$ [GHz]) and the *LTE-3500* ($[f_{2,\min}, f_{2,\max}] = [3.40, 3.60]$ [GHz] $\rightarrow \Delta f_2 = 0.20$ [GHz]) bands ($S_{11}^{th} = -10$ [dB]). The antenna is printed on a dielectric substrate of permittivity $\varepsilon = 3.38$ and loss tangent $\tan\delta = 2.5 \times 10^{-3}$ with thickness $\eta = 0.76$ [mm]. As for the settings of the *PSO-OK/C* synthesis method, the guidelines in the reference literature [27] have been adopted by setting $P = 11$, $I = 100$, and $T_0 = (5 \times K) = 55$.

Figure 2 reports the evolution of the cost function versus the iteration index, clearly indicating the effectiveness of the *SSE* block combined with the adaptively-refined *OK-SM* in reaching the global optimum of the problem at hand. As a matter of fact, a solution with $\Phi\left\{\underline{\chi}\right\} = 0$ has been obtained at the $i = 94$-th iteration ($T_{upd} = 94$ — Fig. 2), indicating that a fully-compliant *PMM* radiator has been obtained with a time saving of $\Delta t \simeq 86\%$ with respect to a standard *PSO* optimization. Such an outcome is verified by the plot of the input reflection coefficient in Fig. 3(c) associated to the optimal solution, whose geometry is shown in Figs. 3(a)–3(b), while the corresponding *DoF*s are reported in Table 1. As it can be noticed, the simulated reflection coefficient is always $S_{11}(f|\underline{\chi}^{(opt)}) < S_{11}^{th}$ for $f \in [f_{1,\min}, f_{1,\max}]$ and $f \in [f_{2,\min}, f_{2,\max}]$ [Fig. 3(c)], thus verifying the desired resonant features. To provide more insights on the *EM* behavior of the synthesized *PMM* radiator, Fig. 4 reports the distribution of the surface current at the center frequency of each target band [i.e., $f_{1,c} = 1.795$ [GHz] — Fig. 4(a); $f_{2,c} = 3.5$ [GHz] — Fig. 4(b)]. As expected, the perturbed Minkowski fractal is differently excited in the two operating bands, with larger values of the surface current occurring in correspondence with the smaller (1-st iteration) details at the highest resonant frequency [Fig. 4(b)]. Finally, the corresponding gain patterns in both bands are plotted in Fig. 5 for the horizontal ($\varphi = 0$ [deg]) plane [Fig. 5(a)] and the two orthogonal vertical cuts [i.e., $\varphi = 90$ [deg] — Fig. 5(b); $\theta = 90$ [deg] — Fig. 5(c)]. The reported results verify that the synthesized antenna properly radiates in both target bands, exhibiting a stable horizontal omnidirectionality [Fig. 5(a)] as well as monopole-like pattern features in the two vertical planes [Figs. 5(b)–5(c)].

To further assess the effectiveness of the *SbD* design methodology as well as to provide a proof of the high flexibility of the proposed *PMM* radiator modeling, let us consider in the following a second benchmark where the high-order resonance must cover the *IEEE-802.11n* standard (i.e., $[f_{2,\min}, f_{2,\max}] = [5.17, 5.835]$ [GHz] $\rightarrow \Delta f_2 = 0.665$ [GHz]), still fitting the *LTE-1800* band in the lowest portion of the spectrum. Regardless of the significant shift of the second band with respect to

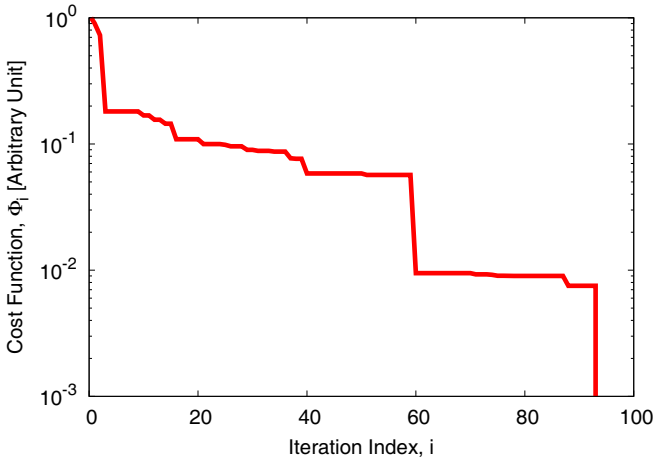

Figure 2. *Numerical Assessment* (*LTE-1800 & LTE-3500 PMM Radiator*, $[f_{1,\min}, f_{1,\max}] = [1.71, 1.88]$ [GHz], $[f_{2,\min}, f_{2,\max}] = [3.40, 3.60]$ [GHz]) — Behavior of the cost function versus the iteration index.

Table 1. *Numerical Assessment* — Optimized values of the geometric *DoF*s for the syntesized *PMM* radiators.

k	χ_k	$\chi_k^{(opt)}$ [mm] Figs. 3(a)-3(b)	$\chi_k^{(opt)}$ [mm] Figs. 6(a)–6(b)
1	H_g	25.50	16.46
2	H_f	24.50	22.00
3	W_{f1}	1.90	1.80
4	W_{f2}	1.97	1.80
5	L_0	25.84	24.85
6	L_1	13.93	5.60
7	L_2	7.00	5.85
8	L_3	10.71	8.51
9	L_4	4.26	10.59
10	L_5	3.72	5.00
11	L_6	7.64	8.66

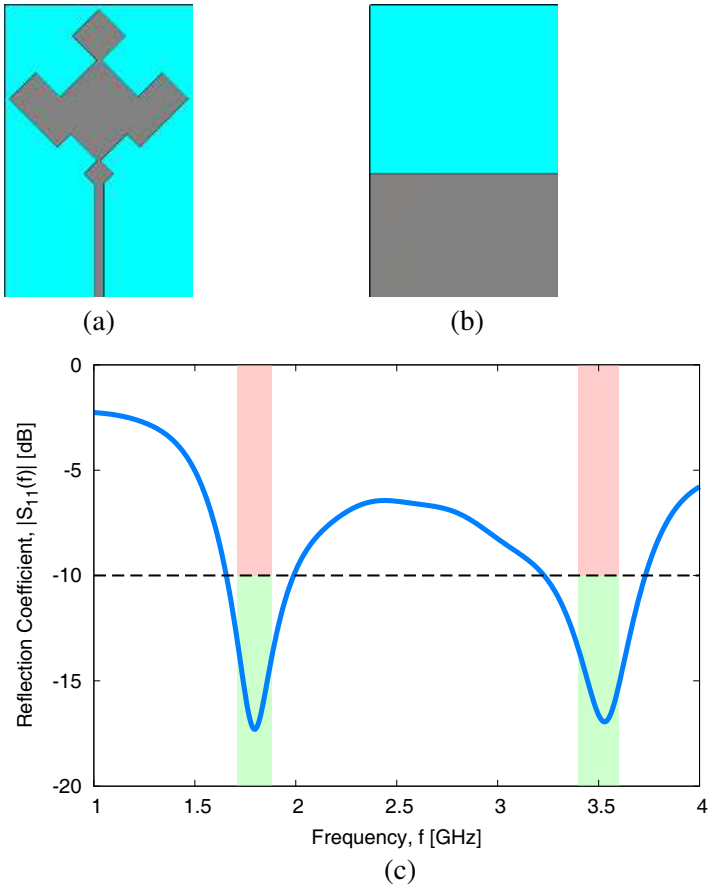

Figure 3. *Numerical Assessment* (*LTE-1800 & LTE-3500 PMM Radiator*, $[f_{1,\min}, f_{1,\max}] = [1.71, 1.88]$ [GHz], $[f_{2,\min}, f_{2,\max}] = [3.40, 3.60]$ [GHz]) — (a) Front and (b) back geometry of the synthesized antenna; (c) behavior of the *FW*-simulated input reflection coefficient versus frequency.

the previous test case (i.e., from $f_{2,c} = 3.5\,[\text{GHz}]$ to $f_{2,c} = 5.5\,[\text{GHz}]$), a proper impedance matching has been achieved by the *SbD* optimized solution [Fig. 6(c)] thanks to the adopted perturbed fractal shaping approach yielding the radiator geometry in Figs. 6(a)–6(b) (Tab. 1). Once again, the simulated gain patterns shown in Fig. 7 on the three main planes verify a proper radiating behavior of the synthesized monopole antenna in both operating bands. As for the total efficiency ν of the optimized design, the simulated values at the two central frequencies are equal to $\nu|_{f=f_{1,c}} = 82\%$ and $\nu|_{f=f_{2,c}} = 78\%$, respectively, being therefore consistent with other microstrip monopole designs found in the recent literarure [38, 39].

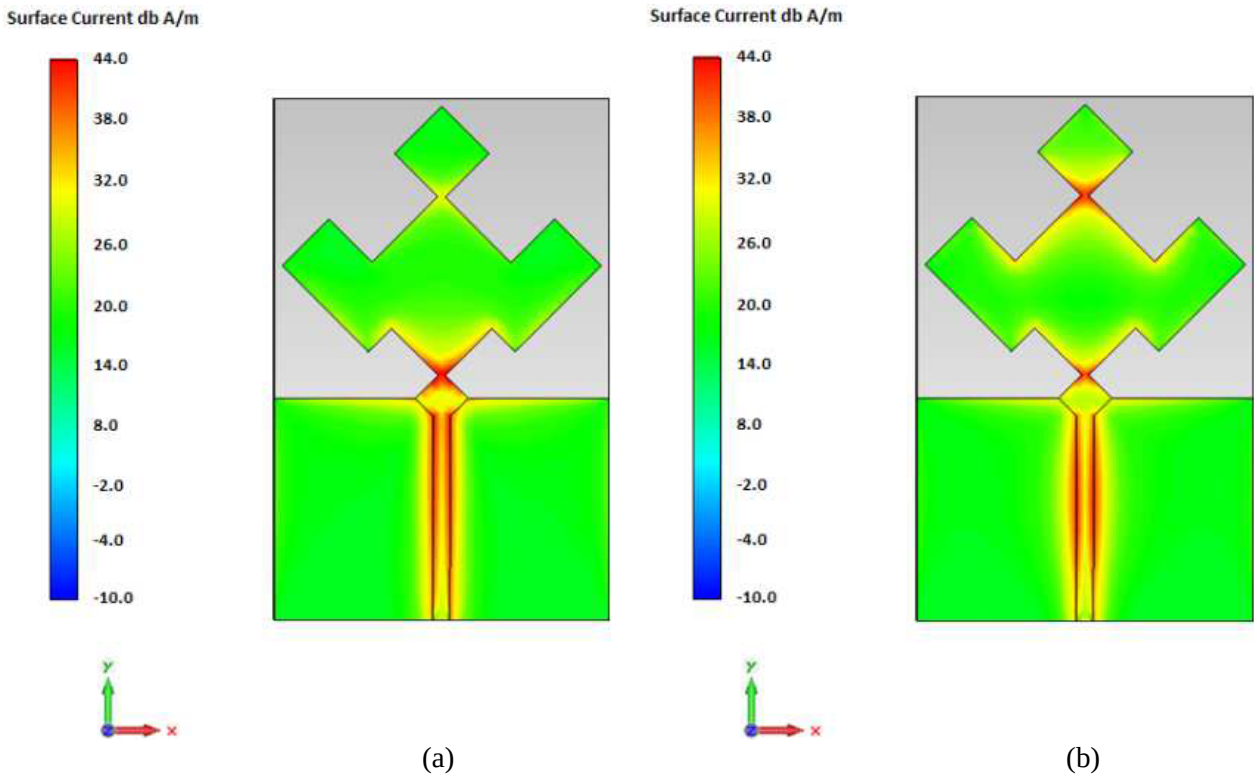

Figure 4. *Numerical Assessment* (*LTE-1800 & LTE-3500 PMM Radiator*, $[f_{1,\min}, f_{1,\max}] = [1.71, 1.88]\,[\text{GHz}]$, $[f_{2,\min}, f_{2,\max}] = [3.40, 3.60]\,[\text{GHz}]$ — *FW*-simulated surface current distribution at (a) $f = f_{1,c} = 1.795\,[\text{GHz}]$ and (b) $f = f_{2,c} = 3.5\,[\text{GHz}]$.

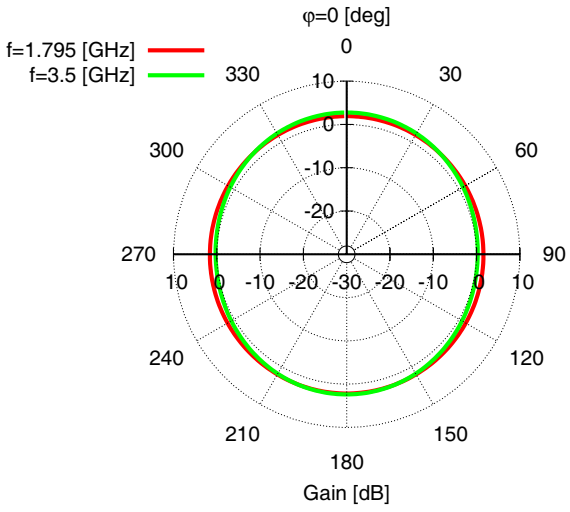

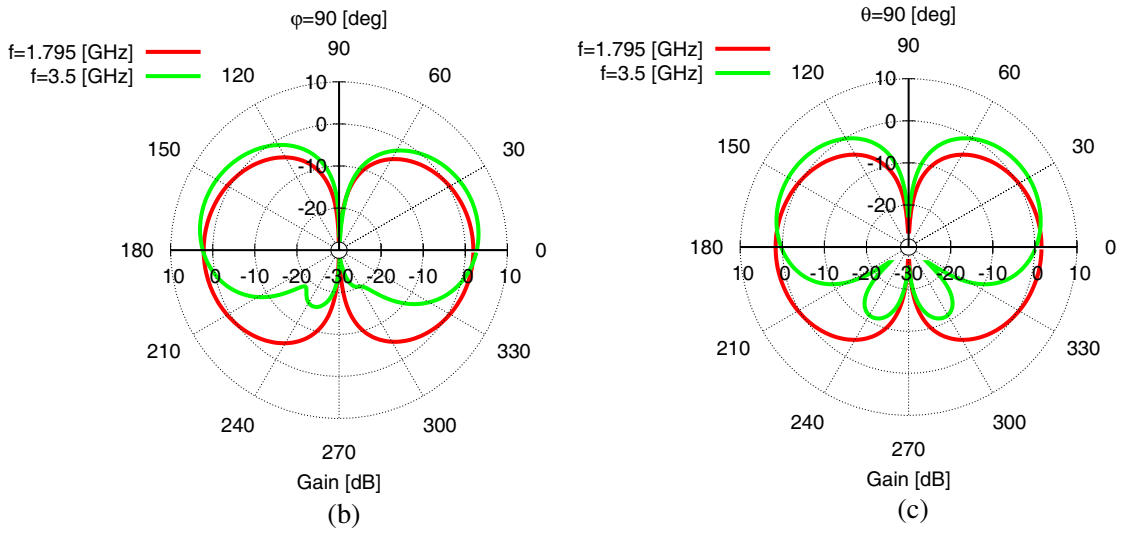

Figure 5. *Numerical Assessment* (*LTE-1800 & LTE-3500 PMM Radiator*, $[f_{1,\min}, f_{1,\max}] = [1.71, 1.88]\,[\text{GHz}]$, $[f_{2,\min}, f_{2,\max}] = [3.40, 3.60]\,[\text{GHz}]$) — *FW*-simulated gain patterns at $f = f_{1,c} = 1.795\,[\text{GHz}]$ and $f = f_{2,c} = 3.5\,[\text{GHz}]$ along the (a) horizontal plane ($\varphi = 0\,[\text{deg}]$), and the vertical planes at (b) $\varphi = 90\,[\text{deg}]$ and (c) $\theta = 90\,[\text{deg}]$.

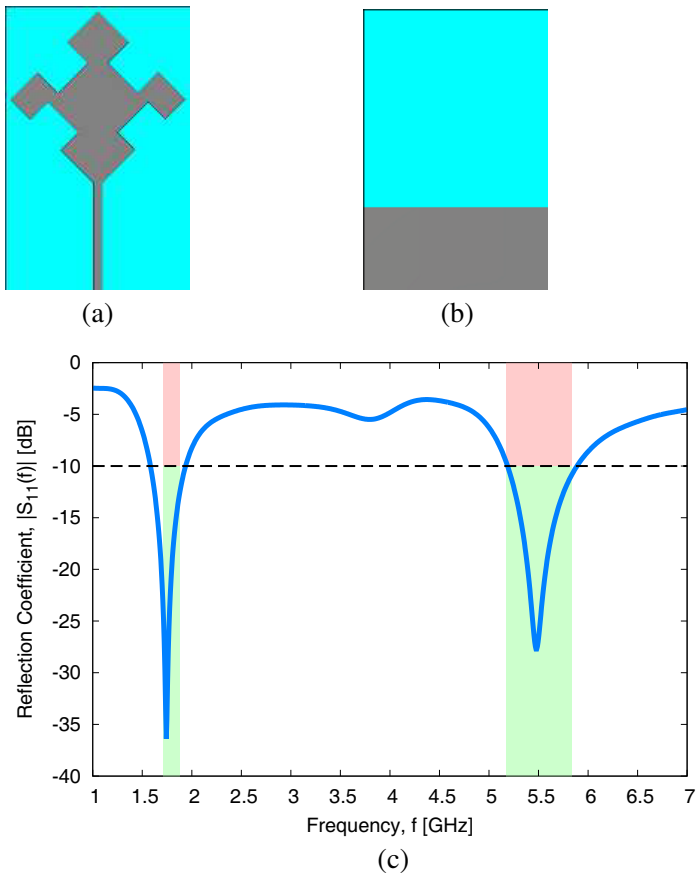

Figure 6. *Numerical Assessment* (*LTE-1800 & IEEE-802.11n PMM Radiator*, $[f_{1,\min}, f_{1,\max}] = [1.71, 1.88]\,[\text{GHz}]$, $[f_{2,\min}, f_{2,\max}] = [5.17, 5.835]\,[\text{GHz}]$ — (a) Front and (b) back geometry of the synthesized antenna; (c) behavior of the *FW*-simulated input reflection coefficient versus frequency.

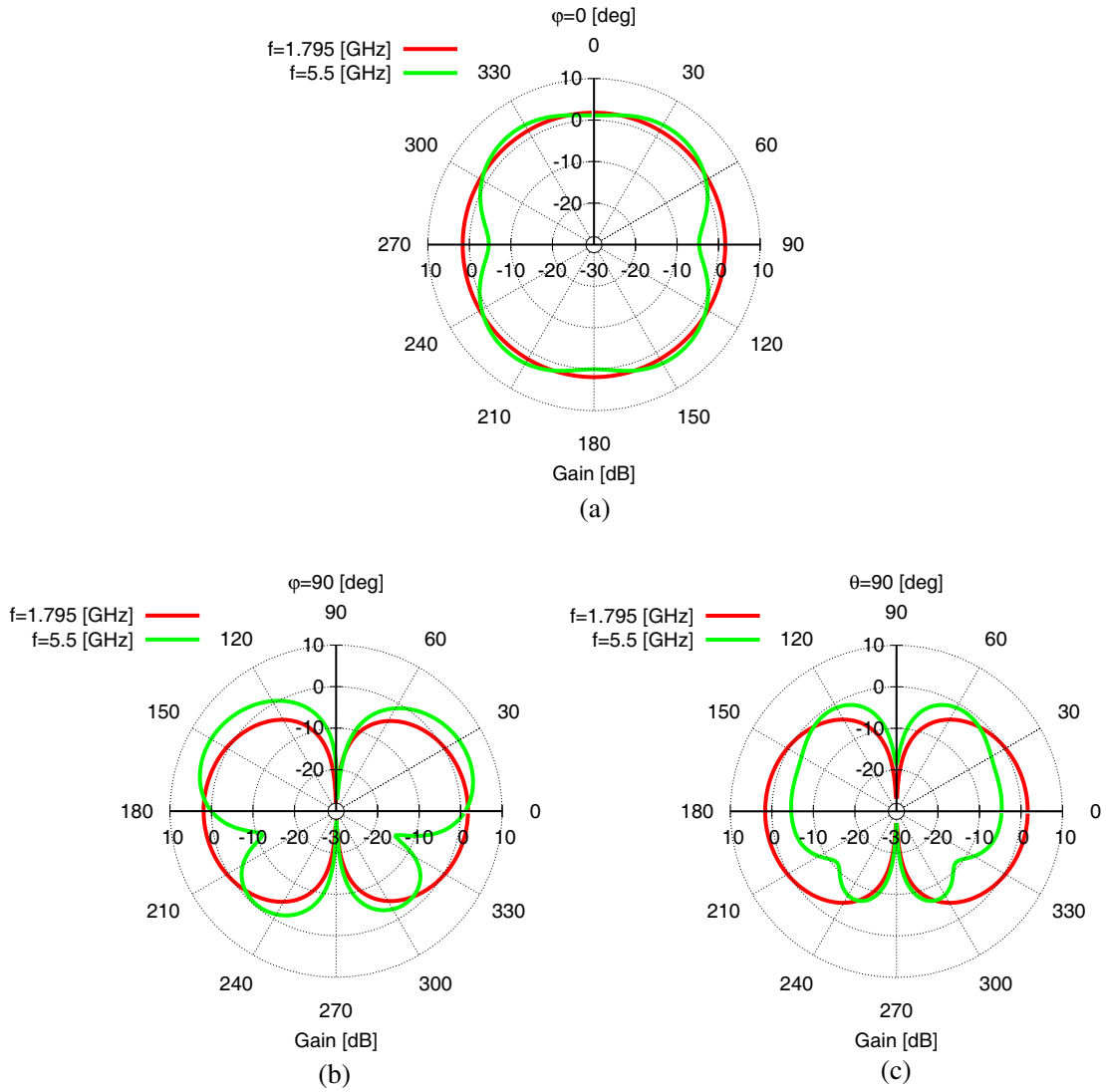

Figure 7. *Numerical Assessment* (*LTE-1800 & IEEE-802.11n PMM Radiator*, $[f_{1,\min}, f_{1,\max}] = [1.71, 1.88]\,[\text{GHz}]$, $[f_{2,\min}, f_{2,\max}] = [5.17, 5.835]\,[\text{GHz}]$) — *FW*-simulated gain patterns at $f = f_{1,c} = 1.795\,[\text{GHz}]$ and $f = f_{2,c} = 5.5\,[\text{GHz}]$ along the (a) horizontal plane ($\varphi = 0\,[\text{deg}]$), and the vertical planes at (b) $\varphi = 90\,[\text{deg}]$ and (c) $\theta = 90\,[\text{deg}]$.

4. CONCLUSIONS

An innovative methodology for the design of dual-band radiators with arbitrarily-tuned resonances has been proposed. It exploits an unconventional modeling of the standard Minkowski fractal relying on a perturbation of the 1-st order insets to overcome the fixed relationship between consecutive resonances of the standard iterative fractal shaping approach. A customized *SbD* technique has been adopted to synthesize *PMM* radiators fitting arbitrary user-defined impedance bandwidth specifications. A high computational time saving with respect to a conventional *PSO*-driven synthesis has been yielded thanks to an on-line adaptively-refined *SM* acting as a fast and accurate digital twin of the time-consuming *FW* solver. The reported numerical results have assessed the effectiveness and flexibility of the proposed *PMM* shaping approach as well as the high efficiency of the adopted *SbD* synthesis engine.

The prototyping and experimental assessment of the designed antennas will be object of future works. Towards this goal, the exploitation of antenna-plexers combining multiple filters to allow several different radios to share a single antenna will be taken into account [40, 41].

ACKNOWLEDGMENT

This work benefited from the networking activities carried out within the Project "MANTLES — Cloaking Metasurfaces for a new Generation of Intelligent Antenna Systems" (Grant No. 2017BHFZKH) funded by the Italian Ministry of Education, University, and Research within the PRIN2017 Program (CUP: E64I19000560001) and the Project "MITIGO — Mitigazione dei rischi naturali per la sicurezza e la mobilita' nelle aree montane del Mezzogiorno" (Grant No. ARS01_00964) funded by the Italian Ministry of Education, University, and Research within the PON R&I 2014–2020 Program (CUP: B64I20000450005).

REFERENCES

1. Goudos, S., I. P. Dallas, S. Chatziefthymiou, and S. Kyriazakos, "A survey of IoT key enabling and future technologies: 5G, mobile IoT, sematic web and applications," *Wireless Personal Communications*, Vol. 97, No. 2, 1645–1675, 2017.
2. Ebling, M., "Pervasive computing and the Internet of Things," *IEEE Pervasive Computing*, Vol. 15, No. 1, 2–4, 2016.
3. Fu, S., X. Zhao, C. Li, and Z. Wang, "A low-profile dual-band dual-polarized dipole antenna for 5G communication applications," *Progress In Electromagnetics Research Letters*, Vol. 104, 131–137, 2022.
4. Jangid, M., Jaiverdhan, S. Yadav, and M. M. Sharma, "A CPW fed cross-shaped dual-band circularly polarized monopole antenna with strip/stub/slot resonator loadings," *Progress In Electromagnetics Research M*, Vol. 109, 113–123, 2022.
5. Wang, W. and G. Sun, "A dual-band circularly polarized antenna with "X" parastic structures," *Progress In Electromagnetics Research Letters*, Vol. 103, 89–97, 2022.
6. Jamshed, M. A., T. W. C. Brown, and F. Héliot, "Dual band two element rim based MIMO antennas with coupling manipulation for low SAR mobile handsets," *Progress In Electromagnetics Research C*, Vol. 119, 125–134, 2022.
7. Anguera, J., A. Andújar, J. Jayasinghe, V. V. S. S. S. Chakravarthy, P. S. R. Chowdary, J. L. Pijoan, T. Ali, and C. Cattani, "Fractal antennas: An historical perspective," *Fractal and Fractional*, Vol. 4, No. 1, 3, 2020.
8. Werner, D. H. and S. Ganguly, "An overview of fractal antenna engineering research," *IEEE Antennas Propag. Mag.*, Vol. 45, No. 1, 38–57, Feb. 2003.
9. Chaudhary, A. K. and M. Manohar, "A modified SWB hexagonal fractal spatial diversity antenna with high isolation using meander line approach," *IEEE Access*, Vol. 10, 10238–10250, 2022.
10. Liu, G., L. Xu, and Z. Wu, "Dual-band microstrip RFID antenna with tree-like fractal structure," *IEEE Antennas Wireless Propag. Lett.*, Vol. 12, 976–978, 2013.
11. Velan, S., E. F. Sundarsingh, M. Kanagasabai, A. K. Sarma, C. Raviteja, R. Sivasamy, and J. K. Pakkathillam, "Dual-band EBG integrated monopole antenna deploying fractal geometry for wearable applications," *IEEE Antennas Wireless Propag. Lett.*, Vol. 14, 249–252, 2015.
12. Peristerianos, A., A. Theopoulos, A. G. Koutinos, T. Kaifas, and K. Siakavara, "Dual-band fractal semi-printed element antenna arrays for MIMO applications," *IEEE Antennas Wireless Propag. Lett.*, Vol. 15, 730–733, 2016.
13. Dhar, S. Ghatak, R., B. Gupta, and D. R. Poddar, "A wideband Minkowski fractal dielectric resonator antenna," *IEEE Trans. Antennas Propag.*, Vol. 61, No. 6, 2895–2903, Jun. 2013.
14. Dhar, S., K. Patra, R. Ghatak, B. Gupta, and D. R. Poddar, "A dielectric resonator-loaded Minkowski fractal-shaped slot loop heptaband antenna," *IEEE Trans. Antennas Propag.*, Vol. 63, No. 4, 1521–1529, Apr. 2015.
15. Salucci, M., N. Anselmi, S. K. Goudos, and A. Massa, "Fast design of multiband fractal antennas through a system-by-design approach for NB-IoT applications," *EURASIP J. Wirel. Comm. Netw.*, Vol. 2019, No. 1, 68–83, Mar. 2019.

16. Viani, F., M. Salucci, F. Robol, G. Oliveri, and A. Massa, "Design of a UHF RFID/GPS fractal antenna for logistics management," *Journal of Electromagnetic Waves and Applications*, Vol. 26, 480–492, 2012.
17. Viani, F., M. Salucci, F. Robol, and A. Massa, "Multiband fractal ZigBee/WLAN antenna for ubiquitous wireless environments," *Journal of Electromagnetic Waves and Applications*, Vol. 26, Nos. 11–12, 1554–1562, 2012.
18. Goudos, S., *Emerging Evolutionary Algorithms for Antennas and Wireless Communications*, SciTech Publishing Inc., Stevenage, 2021.
19. Goudos, S. K., K. Siakavara, T. Samaras, E. E. Vafiadis, and J. N. Sahalos, "Self-adaptive differential evolution applied to real-valued antenna and microwave design problems," *IEEE Trans. Antennas Propag.*, Vol. 59, No. 4, 1286–1298, Apr. 2011.
20. Goudos, S. K., C. Kalialakis, and R. Mittra, "Evolutionary algorithms applied to antennas and propagation: A review of state of the art," *Int. J. Antennas Propag.*, Vol. 2016, 1–12, Jan. 2016.
21. Boursianis, A. D., M. S. Papadopoulou, M. Salucci, A. Polo, P. Sarigiannidis, K. Psannis, S. Mirjalili, S. Koulouridis, and S. K. Goudos, "Emerging swarm intelligence algorithms and their applications in antenna design: The GWO, WOA, and SSA optimizers," *Appl. Sciences*, Vol. 2021, No. 11, 1–27, Sep. 2021.
22. Campbell, S. D., R. P. Jenkins, P. J. O'Connor, and D. Werner, "The explosion of artificial intelligence in antennas and propagation: How deep learning is advancing our state of the art," *IEEE Antennas Propag. Mag.*, Vol. 63, No. 3, 16–27, Jun. 2021.
23. Massa, A., G. Oliveri, M. Salucci, N. Anselmi, and P. Rocca, "Learning-by-examples techniques as applied to electromagnetics," *Journal of Electromagnetic Waves and Applications*, Vol. 32, No. 4, 516–541, 2018.
24. Cui, L., Y. Zhang, R. Zhang, and Q. H. Liu, "A modified efficient KNN method for antenna optimization and design," *IEEE Trans. Antennas Propag.*, Vol. 68, No. 10, 6858–6866, Oct. 2020.
25. Toktas, A., D. Ustun, and M. Tekbas, "Multi-ojective design of multi-layer radar absorber using surrogate-based optimization," *IEEE Trans. Microw. Theory Techn.*, Vol. 67, No. 8, 3318–3329, Aug. 2019.
26. Wu, Q., W. Chen, C. Yu, H. Wang, and W. Hong, "Multilayer machine learning-assisted optimization-based robust design and its applications to antennas and array," *IEEE Trans. Antennas Propag.*, Vol. 69, No. 9, 6052–6057, Sep. 2021.
27. Massa, A. and M. Salucci, "On the design of complex EM devices and systems through the System-by-Design paradigm — A framework for dealing with the computational complexity," *IEEE Trans. Antennas Propag.*, Vol. 70, No. 2, 1328–1343, Feb. 2022.
28. Salucci, M., G. Oliveri, M. A. Hannan, and A. Massa, "System-by-Design paradigm-based synthesis of complex systems: The case of spline-contoured 3D radomes," *IEEE Antennas Propag. Mag.*, Vol. 64, No. 1, 72–83, Feb. 2022.
29. Oliveri, G., A. Gelmini, A. Polo, N. Anselmi, and A. Massa, "System-by-design multi-scale synthesis of task-oriented reflectarrays," *IEEE Trans. Antennas Propag.*, Vol. 68, No. 4, 2867–2882, Apr. 2020.
30. Oliveri, G., M. Salucci, N. Anselmi, and A. Massa, "Multi-scale system-by-design synthesis of printed WAIMs for waveguide array enhancement," *IEEE J. Multiscale Multiphys. Comput. Tech.*, Vol. 2, 84–96, Jun. 2017.
31. Oliveri, G., F. Viani, N. Anselmi, and A. Massa, "Synthesis of multi-layer WAIM coatings for planar phased arrays within the system-by-design framework," *IEEE Trans. Antennas Propag.*, Vol. 63, No. 6, 2482–2496, Jun. 2015.
32. Oliveri, G., A. Polo, M. Salucci, G. Gottardi, and A. Massa, "SbD-Based synthesis of low-profile WAIM superstrates for printed patch arrays," *IEEE Trans. Antennas Propag.*, Vol. 69, No. 7, 3849–3862, Jul. 2021.
33. Oliveri, G., M. Salucci, R. Lombardi, R. Flamini, C. Mazzucco, S. Verzura, and A. Massa, "Wide-angle impedance matching layer-enhanced dual-polarization sub-6 GHz wide-scan array for next generation base stations," *IEEE Trans. Antennas Propag.*, 2022, doi: 10.1109/TAP.2022.3161555.

34. Salucci, M., L. Tenuti, G. Gottardi, M. A. Hannan, and A. Massa, "A System-by-Design method for efficient linear array miniaturization through low-complexity isotropic lenses," *Electron. Lett.*, Vol. 55, No. 8, 433–434, Apr. 2019.
35. Arnieri, E., M. Salucci, F. Greco, L. Boccia, A. Massa, and G. Amendola, "An equivalent circuit/system-by-design approach to the design of reflection-type dual-band circular polarizers," *IEEE Trans. Antennas Propag.*, Vol. 70, No. 3, 2364–2369, Mar. 2022.
36. Oliveri, G., P. Rocca, M. Salucci, and A. Massa, "Holographic smart EM skins for advanced beam power shaping in next generation wireless environments," *IEEE J. Multiscale Multiphys. Comput. Tech.*, Vol. 6, 171–182, Oct. 2021.
37. Oliveri, G., F. Zardi, P. Rocca, M. Salucci, and A. Massa, "Building a smart *EM* environment — *AI*-enhanced aperiodic micro-scale design of passive *EM* skins," *IEEE Trans. Antennas Propag.*, 2022, doi: 10.1109/TAP.2022.3151354.
38. Ghouz, H. H. M., M. F. Abo Sree, and M. Aly Ibrahim, "Novel wideband microstrip monopole antenna designs for WiFi/LTE/WiMax devices," *IEEE Access*, Vol. 8, 9532–9539, 2020.
39. Sediq, H. and Y. Mohammed, "Performance analysis of novel multi-band monopole antenna for various broadband wireless applications," *Wireless Personal Communications*, Vol. 112, No. 1, 571–585, 2020.

40. Contreras-Lizarraga, A., et al., "A high-performance antenna-plexer for mobile devices," *2020 IEEE International Ultrasonics Symposium (IUS)*, 1–3, 2020.
41. QORVO, "Through the 5G antenna design maze with antenna-plexers," 1–7, Oct. 2020. [Online]. Available: https://www.qorvo.com/resources/d/qorvo-through-5g-antenna-design-maze-with-antenna-plexer-white-paper.